PROPERTIES OF MoN_xO_y THIN FILMS AS A FUNCTION OF N/O RATIO

J. Barbosa[1], L. Cunha[1], L. Rebouta[2], C. Moura[1], F. Vaz[2], S. Carvalho[2], E. Alves[3],

E. Le Bourhis[4], Ph. Goudeau[4], J. P. Rivière[4]

[1]Universidade do Minho, Dept. Física, Campus de Gualtar, 4710-057 Braga, Portugal

[2]Universidade do Minho, Dept. Física, Campus de Azurém, 4800-058 Guimarães, Portugal

[3]ITN, Departamento de Física, E.N.10, 2686-953 Sacavém, Portugal

[4]Laboratoire de Métallurgie Physique, Université de Poitiers, 86960 Futuroscope, France

Abstract

The main purpose of this work consists on the preparation of single layered molybdenum oxynitride, MoN_xO_y. The films were deposited on steel substrates by dc reactive magnetron sputtering. The depositions were carried out from a pure Mo target varying the flow rate of reactive gases, which allowed tune the crystallographic structure between insulating oxides and metallic nitrides and consequently electronic, mechanical and optical properties of the material. X-ray diffraction (XRD) results revealed the occurrence of molybdenum nitride for the films with low oxygen fraction: face-centred cubic phases (γ-Mo_2N) for low nitrogen flow rate or cubic MoN_x and hexagonal phase (δ-MoN) for high nitrogen flow rate. The increase of oxygen content induces an amorphization of the nitride phases and appearance of MoO_3 phases. The increase of the oxygen fraction in the films induces also a high decrease in films hardness. Residual stresses revealed to be of compressive type, in the range of very few tenths of GPa to -2 GPa. All these results have been analysed and will be presented as a function of the deposition parameters, the chemical composition and the structure of the films.

1. Introduction

Metal oxynitride films represent a group of modern ceramic materials of increasing technological importance. These materials show a wide variety of optical, electrical and mechanical properties providing some opportunities for technological applications. Their importance results from the presence of oxygen that allows the tailoring of film properties between those of "pure" covalent nitride and the correspondent largely ionic oxides. Recently transition metal oxynitrides have been investigated, mainly zirconium and titanium oxynitrides, however the preparation and investigation of molybdenum oxynitride is not so intensive.

Thin films of molybdenum nitride present interesting properties that made them a material to be used as diffusion barriers [1,2,3] and as catalyst [4,5]. Molybdenum nitride coatings also present good tribological [6, 7] and superconducting [8] properties. A variety of techniques have been used to produce polycrystalline and amorphous molybdenum nitride thin films, such as reactive magnetron sputtering [2,3,9,10], chemical vapour deposition (CVD) [1], pulsed laser deposition (PLD) [11], arc PVD [12], ion-beam deposition and ion implantation [13 e 14].

Molybdenum trioxide has been used has catalyst in oxidation of hydrocarbons or reduction of NO_x [15,16]. S. S. Sunu et all studied the electrical conductivity and gas sensing properties of molybdenum trioxide [17].

There has been some investigation of physisorption and chemisorption of molybdenum oxynitride [18], or as catalyst [19,20] but to our knowledge there is only one work devoted to the effect of oxygen on structural properties of molybdenum oxynitride (MoO_xN_y) thin films[21]. The investigation of the structural arrangements of single layered molybdenum oxynitride, MoN_xO_y, is not straightforward since the phase formation of these systems is correlated with the deposition conditions. Moreover Mo-N systems have several stable bulk phases, face centred cubic (γ-phase), face centred tetragonal and hexagonal phase

(δ-phase), strongly dependent of nitrogen partial pressure in the chamber, that add some complexity to the analysis of the structural and mechanical properties of the produced films.

2. Experimental details

The MoN_xO_y samples were deposited by reactive dc magnetron sputtering. The deposition system consists of two vertical rectangular magnetrons (unbalanced of type 2), in a closed field configuration. Polished high-speed steel (AISI M2) and stainless substrates were used for depositions, after ultrasonic cleaning and sputter etched for 15 min in an Ar atmosphere. Depositions were carried out using only one magnetron under an $Ar/(N_2+O_2)$ atmosphere, in static mode and the target to substrate distance was maintained constant (70 mm). The Ar flow was about 55 sccm in all depositions, which correspond to a partial pressure of 0.4 Pa. For comparison purposes, molybdenum oxide and molybdenum nitride samples were prepared, using an oxygen flow of 18.5 sccm and a nitrogen flow of 20 sccm, respectively. The d.c. power density applied at the molybdenum target was kept constant at 75 $A.m^{-2}$. The molybdenum oxinitride samples were prepared using a d.c. current density of 37.5 $A.m^{-2}$ in the molybdenum target and with a total reactive gas flux (N_2+O_2) of 60 sccm, with nitrogen flows from 50 to 60 sccm and oxygen flows up to 10 sscm. The two reactive gases were introduced in the chamber using two different mass flow controllers, except in the case of low oxygen flows. In this case it was used a nitrogen flow plus a gas mixture (O_2+N_2) with 15% of oxygen. The base pressure in the deposition chamber was about 10^{-4} Pa and raised to values around 1 Pa during depositions, for a total reactive gas flux of 60 sccm. An external heating resistance positioned at 8 cm from the substrate holder was used to heat the samples.

The chemical composition of the films was determined by Rutherford backscattering spectrometry (RBS), using a 1 MeV $^1H^+$ beam. The RUMP code [22] was used to extract the information from the RBS spectra. An average number of 5 ball cratering (BC) experiments were carried out in each sample in order to determine its thickness. The crystallographic

structure was investigated by X-ray diffraction in a conventional θ/2 θ configuration, using a monochromatic Cu Kα radiation. The coating hardness and Young's modulus were determined from the loading and unloading curves, carried out with an ultra low load-depth sensing Berkovich nanoindenter from CSM Instruments (Switzerland). A Poisson's ratio of 0.3 was used for the calculations. The maximum load used was 30 mN, with a loading time of 30 s, holding 30 s and unloading in 30 s, producing an average number of 15 indentations per sample. Residual stresses, σ_r, were taken from Stoney equation [23], using substrate curvature radii, both before and after coating deposition [24].

3. Results and Discussion

3.1. Deposition rate and chemical composition

The nitrogen and oxygen contents of the samples, extracted from RBS experiments, were normalized to the molybdenum content. The indexes of nitrogen and oxygen will be noted in the text and figures as x and y, respectively. The oxygen fraction was determined by the ratio of the oxygen content and the sum of both oxygen and nitrogen contents: $f_O = c_O/(c_O+c_N)$.

The variation of the deposition rate with oxygen flow (for a constant total flow of both reactive gases, O_2 and N_2, of 60 sccm) is plotted in Figure 1: This plot shows an increasing deposition rate with the increase of the oxygen flow, from 2.7 μm/h for a pure nitride, to 3.7 μm/h when an oxygen flow of 10 sccm is used. The increase of oxygen partial pressures promotes target poisoning and the reactive sputtering of metals usually shows a significant decrease in the deposition rate when it changes from the metallic mode to the compound mode. However, in the present case, and for a partial pressure of the both reactive gases of about 0.35 Pa, the nitrided/oxidized layer on top of the target is still an electrical conductive material and a decrease in the deposition rate should be obtained only for an higher reactive gas flow. The molybdenum nitride/oxide resistivity changes slowly with the partial reactive gas pressure and for a broad range, which allows a wide variation of the target potential, as

shown in Fig. 2. A similar increase in the deposition rate, as a function of the reactive gas pressure, followed by a significant decrease in the deposition rate was also reported by Kharrazi et al [25]. The evolution of deposition rate with the reactive gas flow is well correlated with the change of the concentration of non-metallic elements, x + y (Fig. 1), which suggests that the initial increase is related with the addition of the non metallic elements.

The increase of oxygen partial pressure maintaining the total pressure, resulted in a higher oxygen fraction in films composition, as expected. Molybdenum reactivity with reactive gases is significantly lower when compared with other transition metals (Ti, Zr …). In order to produce molybdenum nitride it is necessary a higher partial pressure of nitrogen inside the deposition chamber. This is due to the low heat of formation of molybdenum nitride when compared to heat of formation of the transition metal nitrides of group IV [2]. However, oxygen is much more reactive than nitrogen and we could obtain an oxygen fraction of 0.83 in film composition for only 21% of fraction of oxygen (relatively to N_2 + O_2) in deposition chamber (see Figures 1 and 2).

3.2. Structural properties

For comparison purposes, Molybdenum nitride samples were prepared with different nitrogen flows. The sample produced with a nitrogen flow of 20 sccm (partial pressure of 0.07 Pa) presents diffraction peaks corresponding to a fcc phase with a lattice parameter of 0.418 nm, which can be assigned to the γ-Mo_2N phase (ICDD card 25-1366), as shown on Fig.3a. This crystal structure is a NaCl-type structure where Mo atoms are occupying fcc sites and N atoms occupy 50% of octahedral sites [26].

Increasing the nitrogen flow (50 sccm - partial pressure of 0.3 Pa), the formation of a stoichiometric molybdenum nitride with about 52 at.% of nitrogen was induced. All the peaks are shifted to lower diffraction angles when compared to unconstrained γ-Mo_2N (Fig. 3b), and can be indexed to a NaCl-type B1 cubic structure with a lattice parameter of 0.427 nm. This

metastable cubic MoN phase has a higher lattice constant as a result of the nitrogen incorporation into the fcc phase, and this increase of the lattice parameter (0.419 – 0.427 nm) with increasing nitrogen contents (MoN_x, $0.9 < x < 1.3$) was already reported by Linker et al [1] and by Perry et al [27]. The 50% vacant octahedral sites of γ-Mo_2N phase may be preferential occupied by the excess of nitrogen, but the nitrogen atoms may also occupy interstitial sites, resulting in the lattice expansion [2]. However, a small peak at about 35º, suggests also the presence of the hexagonal δ-MoN (ICCD card 25-1367). This peak cannot be addressed to the fcc cubic phase and was already reported and identified as belonging to the hexagonal δ-MoN phase [12]. This hexagonal δ-MoN phase is usually formed for high nitrogen pressures, which supply the necessary high nitrogen content of this phase [12].

The high reactivity of oxygen promoted significant changes in films structure. The addition of an oxygen flow of 4 sccm to the nitrogen flow used for the formation of the γ-Mo_2N phase also induced a shift of the Bragg diffraction lines towards to lower 2θ angles (meaning a higher lattice parameter (0.427 nm)), maintaining the same B1 type structure (Fig. 3c). This behavior cannot be explained by an oxide formation, and the nitrogen content does not justify the increase of the lattice parameter, suggesting that some oxygen is incorporated into the γ-Mo_2N phase. Part of the oxygen atoms occupy the 50% vacant octahedral sites of stoichiometric γ-Mo_2N, resulting in an expansion of the lattice. The stoichiometric ratio in MoN_x compound can be larger than 1, and a x value as high as 1.7 was already reported [8]. Volpe et all [28] and Robertson et all [29] refer the formation of an intermediate phase: MoO_xN_{1-x}.

Figure 4 shows the X-ray diffraction patterns of the samples produced with increasing O_2 flow (increasing oxygen content in the films), but maintaining constant the total reactive gases flow ($O_2 + N_2$) and the other deposition parameters. The increase of oxygen fraction provokes the decrease of the grain size of the molybdenum nitride crystallites (oxygen flows up to 5 sccm), as shown in Fig 4b-d by the broadening of diffraction lines. With the introduction of

an oxygen flow of 1.5 sccm (Fig. 4b), the XRD pattern shows a broad peak around $2\theta \approx 36.0^{\circ}$, which is shifted to lower diffraction angles when compared to one in cubic MoN_x, $2\theta \approx 36.4^{\circ}$ (Fig 4a). However, the peak at $2\theta \approx 42.4^{\circ}$ (Fig 4b) is slightly shifted to higher diffraction angles. This suggests that the peak at $2\theta \approx 36.0^{\circ}$ can be indexed to the [200] direction of the hexagonal δ-MoN phase (JCPDS card number 25-1367). The small peak $2\theta \approx 74.3^{\circ}$, cannot be indexed to the cubic MoN_x, and may be assigned to the [222] direction of the hexagonal δ-MoN phase. The small shift of the peak at $2\theta \approx 42.4^{\circ}$ to higher diffraction angles corresponds to a decrease in the lattice parameter of the cubic MoN_x, phase. Although only for molybdenum nitride phases, and when the increase in the nitrogen partial pressure induced the growth of the hexagonal δ-MoN phase in coexistence with the cubic phase, a decrease in the lattice parameter of this cubic phase was already reported by Hones et al [30]. This lattice parameter decrease can be explained by the vacancy/interstitial diffusion between the coexisting phases, which means that nitrogen vacancies in the hexagonal δ-MoN matrix diffuse towards the cubic MoN_x [30]. In the present study, these changes are induced by the introduction of the oxygen flow, which suggests that the oxygen plays the role of the excess of nitrogen in the case that only nitrogen reactive gas is used.

With oxygen flows higher than 5 sccm, the oxygen content in the film becomes predominant and the nitride diffraction peaks disappear in the XRD patterns (Fig.4e-g), and it is detected an amorphization of the films. The peaks corresponding to this oxide phase are not well defined, because there is always a strong partial pressure of nitrogen during the deposition, allowing the insertion of nitrogen atoms in the oxide structure. A broad band grows in the range $20^{\circ} < 2\theta < 30^{\circ}$, as oxygen fraction increases. The angular position of the most intense peaks of molybdite (orthorhombic MoO_3, ICCD card number 5-508) and of the monoclinic phase of MoO_3 (ICCD card number 47-1329) are inside this range. At the range $48^{\circ} < 2\theta < 60^{\circ}$ also appears a broad band, less intense than the former. This is also a region

where several less intense diffraction peaks of the orthorhombic and monoclinic phases of MoO_3 are located according to ICDD cards.

The XRD pattern of the Mo oxide sample prepared with a oxygen flow of 20 sccm, presents broad peaks, probably due to relatively high oxygen partial pressure during deposition, but also reveals a strong line around $2\theta \approx 22.6^{\circ}$, which can be indexed to orthorhombic MoO_3 phase, to the monoclinic MoO_3 phase (JCPDS card number 47-1081) or to the metastable tetragonal $MoO_{2.80}$ phase (JCPDS card number 12-517). Small peaks located around the diffraction angles of 27.1º, 46.4º, 49.1º and 53.1º can be addressed to both the orthorhombic MoO_3 phase or to the monoclinic MoO_3 phase. The stoichiometry ratio of this sample, measured by RBS, is about 2.8.

3.3. Hardness and residual stress

The transition from nitride to oxide phase has strong consequence in mechanical properties (Fig. 5). There is a strong decrease in hardness and elastic modulus as the oxygen content increases. It is evident a transition from nitride to oxide phases at an oxygen flow rate around 5 sccm. Pure molybdenum nitride revealed the highest hardness value (~25 GPa), and samples where nitride XRD diffraction lines are still present showed hardness values higher than 15 GPa. A remarkable hardness decrease is revealed for samples with higher oxygen fraction (>70%), which show hardness values lower than 5 GPa.

Figure 6 shows the residual stress of the samples as a function of the oxygen flow and evidences even more clearly than figure 5 the transition between nitride and oxide phases. In the range from pure MoN_x to Mo oxynitride obtained with an oxygen flow of 5 sccm, the samples revealed a compressive residual stress with values around -1.5 GPa. In accordance with hardness values, this is also the range where nitride diffraction lines are still present in XRD patterns. The incorporation of nitrogen and oxygen into the cubic MoN_x phase induced structural defects resulting in a lattice expansion, which justifies the compressive residual

stress for relatively high oxygen content. For higher oxygen content, a dramatic decrease in the compressive residual stress was observed, which coincides with the film amorphization.

4. Conclusions

Thin films within the Mo-N-O ternary system were prepared by dc reactive magnetron sputtering. Structural characterization results reveal a strong dependence of the film texture on the oxygen fraction. The samples produced with nitrogen as reactive gas reveal the presence of fcc γ-Mo_2N or cubic MoN_x and h-MoN for low or high N_2 flow rate, respectively. The increase of oxygen partial pressure starts to decrease the grain size increase and, for higher partial pressure, induces the amorphization of the film and the appearance of orthorhombic or monoclinic phases of MoO_3.

Hardness, Young's modulus and residual stress measurements revealed a strong decrease with increase of oxygen fraction in the films.

Acknowledgements

The authors are grateful to the financial support of the FCT institution by the project nº POCTI/CTM/38086/2001 co-financed by European community fund FEDER.

References

1. S.L. Robertson, D. Finello, R.F. Davies, Surface and Coatings Technologies 102 (1998) 256.
2. V.P. Anitha, S. Major, D. Chandrashekharam, Mukesh Bhatnagar, Surface and Coatings Technologies 79 (1996) 50-54.
3. Jui-Chang Chuang, Shuo-Lun Tu, Mao-Chie Chen, Thin Solid Films 346 (1999) 299-306.
4. S. Li, J. S. Lee, J. Catalysis 173 (1998) 134.
5. S. Li, J. S. Lee, J. Catalysis 178 (1998) 119.
6. M. Ürgen, O.L. Eryilmaz, A.F. Cakir, E.S. Kayali, B. Nilüfer, Y. Isik, Surf. Coat. Technol. 94/95 (1997) 501.

7. K.W.Kreutz, M. Krosche, H. Sung, A. Voss, Surf. Coat. Technol. 53 (1992) 57.

8. G. Linker, R. Smithey, O. Meyer, J.Phys. F: Met Phys. 14 (1984) L115.

9. Y. G. Shen, Materials Science and Engineering A359 (2003) 158.

10. Yimin Wang, Ray, Y. Ling, Materials Science and Engineering B 112 (2004) 42.

11. M. Bereznai, Z. Tóth, A.P. Caricato, M. Fernández, A. Luches, G. Majni, P. Mengucci, P.M. Nagy, A. Juhász, L. Nánai, Thin Solid Films *in press*

12. M.K. Kazmanli, M.Urgen, A.F.Cakir, Surf. Coat. Technol. 167 (2003) 77.

13. J.D. O'Keefe, C.H. Skeen, J. Appl. Phys. 44 (1973) 4622

14. B.P. Fairand, B.A. Wilcox, W.J. Gallagher, D.N. Williams, J. Appl. Phys. 64 (1993) 81.

15. D.B. Dabyburjor, S.S. Jewar, E. Ruckenstien, Cat. Rev.-Sci. Eng. 19 (1979) 293.

16. .A. Larrubia, G. Ramis, G. Busca, Appl. Catal. B: Environ. 27 (2000) L145.

17. S.S. Sunu, E. Prabhu, V. Jayaraman, K.I. Gnanasekar, T.K. Seshagiri, T. Gnanasekaran, Sensors and Actuators B 101 (2004) 161.

18. C. Sayag, G. Bugli, P. Havil, G. Djéga-Mariadassou, J. Catalysis 167 (1997) 372.

19. Thierry Bécue, Jean-Marie Manoli, Claude Potvin, Gérald Djéga-Mariadassou, J. Catalysis 170 (1997) 123.

20. P. Perez-Romo, C. Potvin, J.-M. Manoli, G. Djéga-Mariadassou, J. Catalysis 208 (2002) 187.

21. Y.G. Shen, Yiu-Wing Mai, Materials Science and Engineering B 95 (2002) 222.

22. L. R. Doolittle, Nucl. Inst. and Meth. B9 (1985) 344.

23. G. G. Stoney, Proc. Roy. Soc. (London) [A] 82 (1909) 172.

24. F. Vaz, L. Rebouta, P. Goudeau, J. P. Rivière, M. Bodmann, G. Kleer and W. Döll, Thin Solid Films 402 (2002) 195.

25. M. Kharrazi, A.Azen, L.Kullman, C.G.Granqvist, Thin Solid Films 295 (1997) 117.

26. H. Jehn, P. Ettmayer, J. Less-Common Met., 58 (1978) 85.

27. A. J. Perry, A.W. Baouchi, J.H. Petersen, S.D. Pozder, Surf. Coat. Technol. 54/55 (1992) 261.

28. L. Volpe, M. Boudart, J. Solid State Chem. 59 (1985) 332.

29. S. L. Robertson, D. Finello, R.F. Davis, Materials Science and Engineering A248 (1998) 198-205.

30. P. Hones, N. Martin, M. Regula, F. Lévy, J. Phys. D: Appl. Phys. 36 (2003) 1023.

Figure captions

Figure 1. Deposition rate of the deposited films and the nitrogen and oxygen content as a function of oxygen flow. For this set of samples the total reactive gas flow (60 sccm) and substrate bias voltage (-50 V) were maintained during deposition.

Figure 2. Target potential and oxygen fraction in the deposition chamber as function of oxygen flow during depositions. For this set of samples the total reactive gas flow (60 sccm) and substrate bias voltage (-50 V) were maintained during deposition.

Figure 3. XRD patterns of molybdenum nitride and molybdenum oxynitride prepared at different reactive gas flow: a) 20 sccm N_2; b) 50 sccm N_2 ; c) 21 sccm N_2 + 4 sccm O_2

Figure 4. XRD patterns of MoN_xO_y films with different oxygen fractions. The peak located at $2\theta \approx 22.6$ for pure oxide coating may be assigned to orthorhombic, monoclinic MoO_3 or tetragonal $MoO_{0.28}$.

Figure 5. Hardness and Young's modulus of sputtered MoN_xO_y films, measured by nanoindentation technique, as a function of the oxygen flow, maintaining constant the total reactive gas flow (O_2+N_2) in 60 sccm.

Figure 6. Residual stress of sputtered MoN_xO_y films as a function of the oxygen flow, maintaining constant the total reactive gas flow (O_2+N_2) in 60 sccm.

Fig. 1

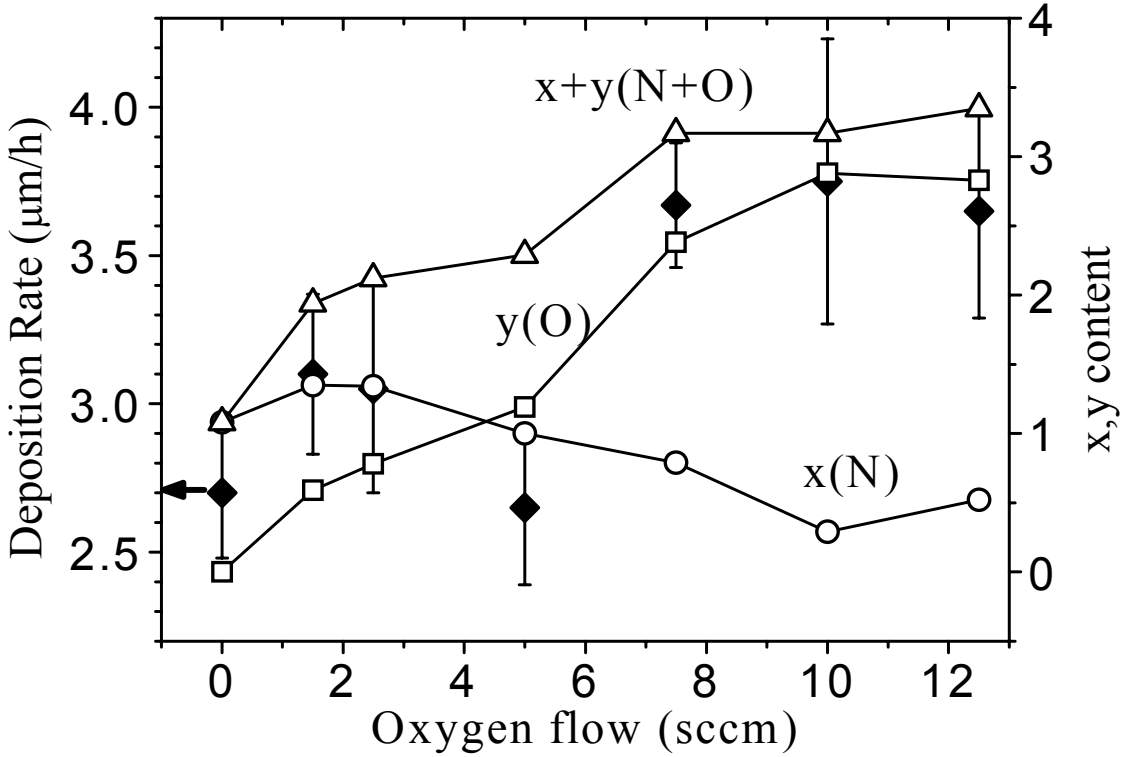
Deposition Rate (μm/h)
x,y content
Oxygen flow (sccm)
x+y(N+O)
y(O)
x(N)
4.0
3.5
3.0
2.5
0
2
4
6
8
10
12
4
3
2
1
0

Fig. 2

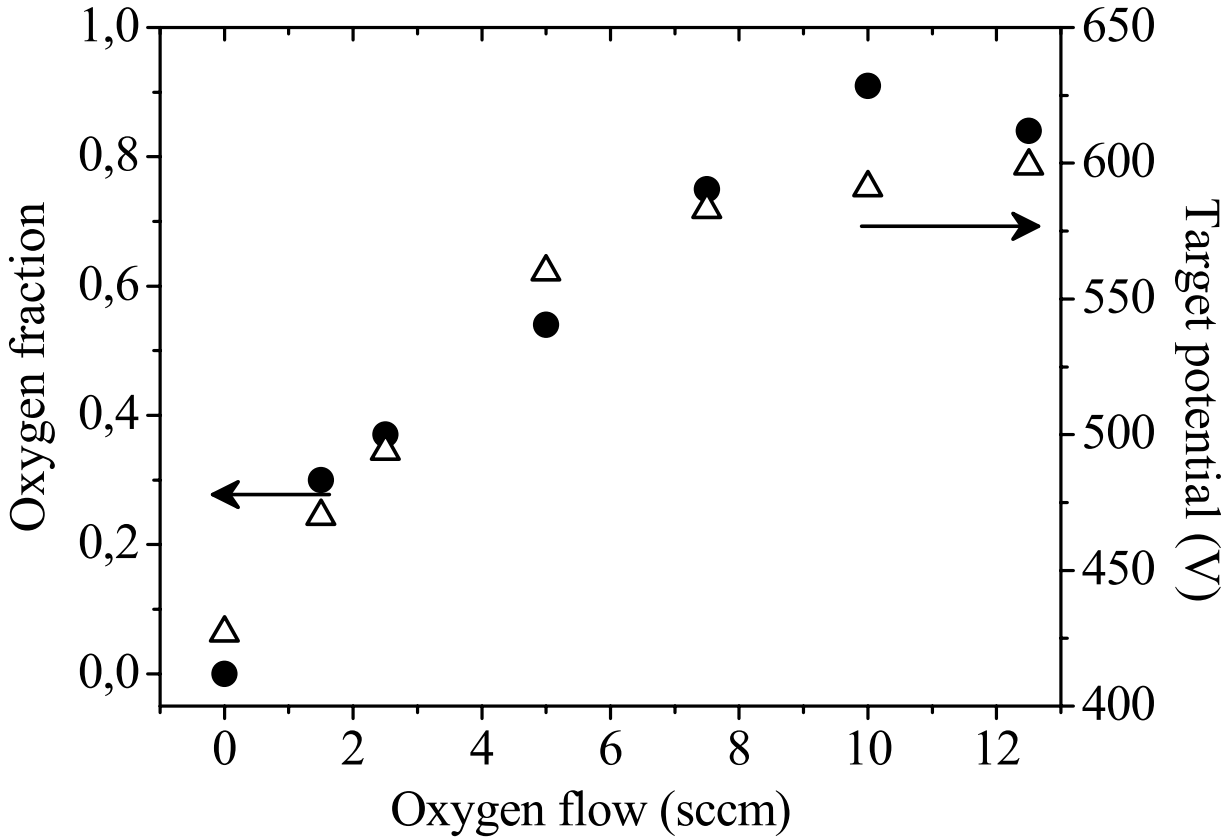
1,0
0,8
0,6
0,4
0,2
0,0
Oxygen fraction
650
600
550
500
450
400
Target potential (V)
0
2
4
6
8
10
12
Oxygen flow (sccm)

fig. 3

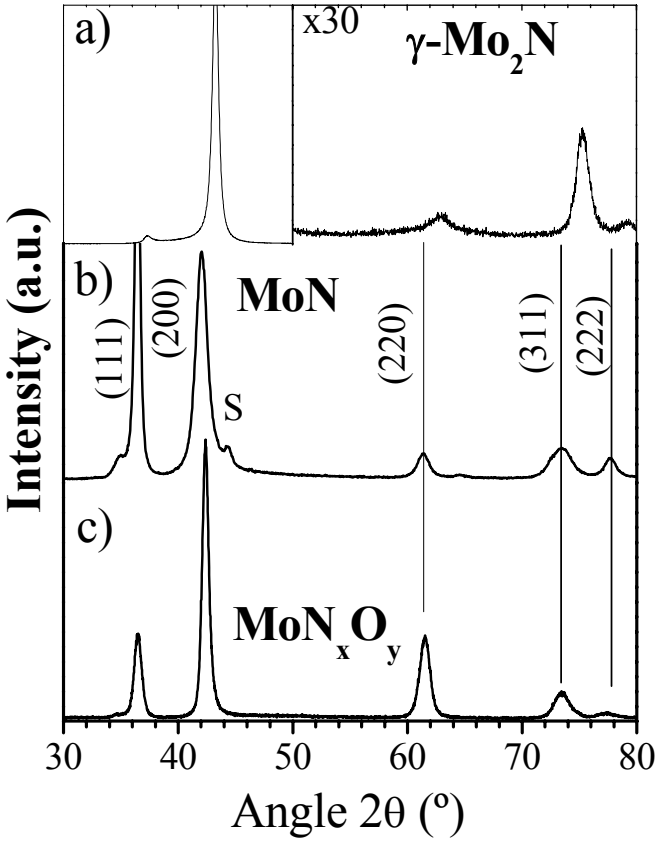
a)
x30
γ-Mo2N
b)
MoN
(111)
(200)
S
(220)
(311)
(222)
c)
MoNxOy
Intensity (a.u.)
30
40
50
60
70
80
Angle 2θ (º)

fig. 4

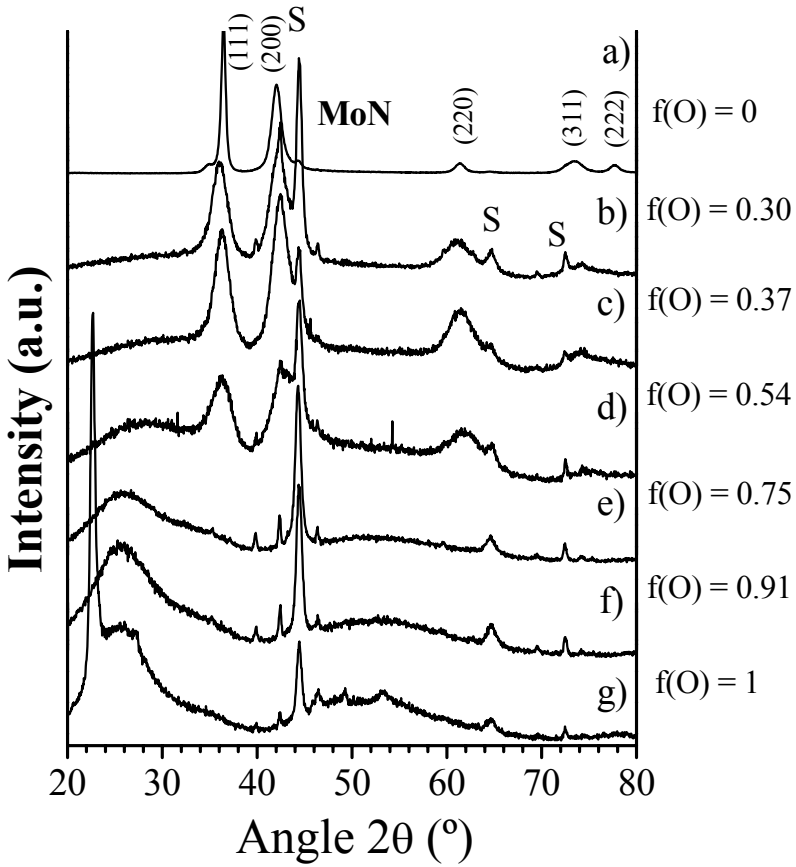
(111)
(200)
S
a)
MoN
(220)
(311)
(222)
f(O) = 0
S
S
b)
f(O) = 0.30
c)
f(O) = 0.37
d)
f(O) = 0.54
e)
f(O) = 0.75
f)
f(O) = 0.91
g)
f(O) = 1
Intensity (a.u.)
20
30
40
50
60
70
80
Angle 2θ (º)

Fig. 5

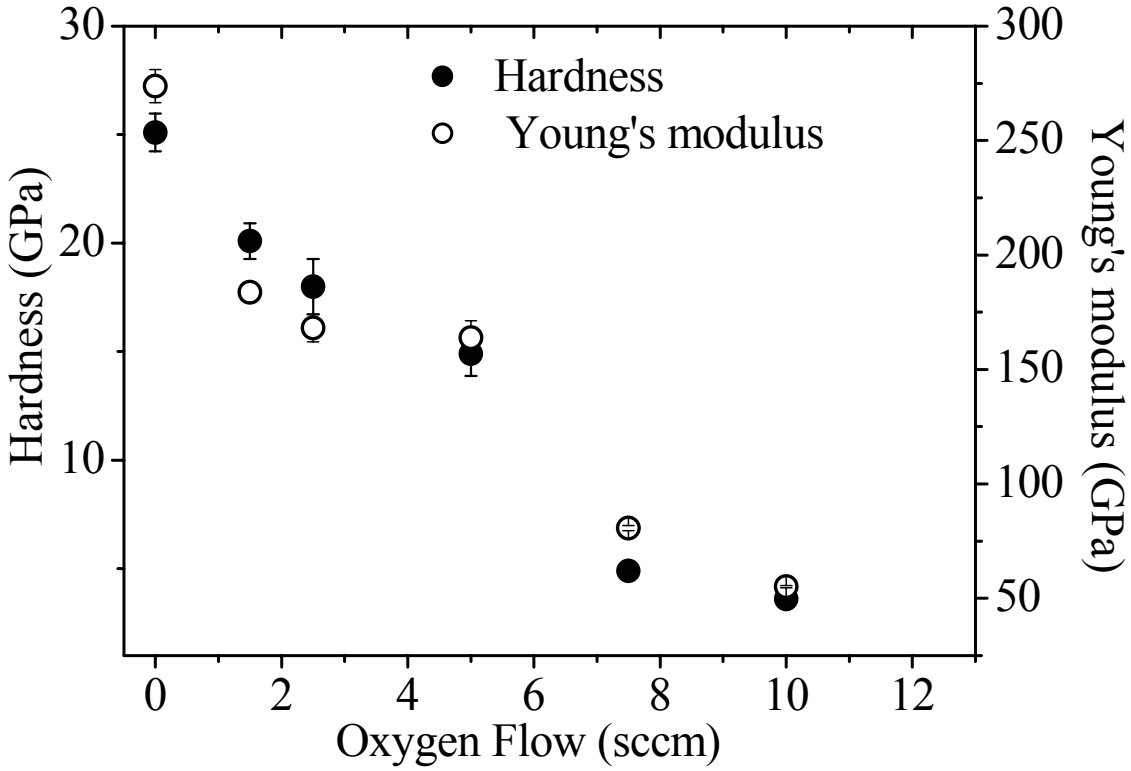
Hardness
Young's modulus
Hardness (GPa)
Young's modulus (GPa)
Oxygen Flow (sccm)
30
20
10
300
250
200
150
100
50
0
2
4
6
8
10
12

Fig. 6